*Physiol Genomics* 29: 84–90, 2007.
First published November 28, 2006; doi:10.1152/physiolgenomics.00305.2005.

# Characterization of circulatory disorders in β-thalassemic mice by noninvasive ultrasound biomicroscopy

**Ekatherina Stoyanova,[1] Marie Trudel,[2] Hady Felfly,[2] Damien Garcia,[2] and Guy Cloutier[1]**

[1]*University of Montreal Hospital Research Center and* [2]*Clinical Research Institute of Montreal, Montreal, Quebec, Canada*

Submitted 12 December 2005; accepted in final form 21 November 2006

**Stoyanova E, Trudel M, Felfly H, Garcia D, Cloutier G.** Characterization of circulatory disorders in β-thalassemic mice by noninvasive ultrasound biomicroscopy. *Physiol Genomics* 29: 84–90, 2007. First published November 28, 2006; doi:10.1152/physiolgenomics.00305.2005.—β-Thalassemia is an inherited hematological disease caused by a decrease or absence of production of β-globin that requires chronic therapeutic interventions. This condition leads to important arterial and venous thromboembolic events, transitory ischemic attacks, and microcirculatory obstructions, indicative of circulatory disturbances. To investigate the presence of microcirculatory disorders without the confounding effect of treatments, we used β-thalassemic mice with typical clinical characteristics of human β-thalassemia major. One impediment to the understanding of microcirculatory physiology, in particular for β-thalassemic mice, has been the lack of an appropriate noninvasive imaging approach. We thus developed a novel noninvasive high-frequency ultrasound imaging method to evaluate murine vascular hemodynamic properties. In our β-thalassemic mice, total peripheral vascular resistance was significantly increased ($P < 0.01$) compared with wildtype littermates, whereas mean blood pressure, heart rate, and cardiac output were similar ($P$ = nonsignificant). Importantly, the vascular hemodynamics in β-thalassemic mice were significantly affected according to the Pourcelot indexes measured in the common carotid artery and abdominal aorta ($P < 0.01$ and $P < 0.05$, respectively). Hence, our β-thalassemia characterization of vascular hemodynamics by noninvasive ultrasonic approaches proves the existence and provides unique quantitative assessment of microcirculatory flow disturbances in those mice.

high-frequency ultrasonography; vascular resistance; blood flow; hemodynamics

THALASSEMIA SYNDROMES ARE a group of heterogenous hereditary diseases characterized by a decrease or a total absence of synthesis of α- and/or β-globin chains composing the hemoglobin protein in red blood cells (RBCs) (29). They are classified according to the type of deficient globin chain as α- and β-thalassemia (30). In β-thalassemia, the severity of the pathophysiology depends on the level of β-globin chain deficiency, which leads to an excess of α-globin chains (32). Consequently, thalassemic RBCs are hypochromic and microcytic and have a shorter half-life, leading to anemia (9).

β-Thalassemia is encountered worldwide, with a higher incidence in the Mediterranean region, Africa, the Middle East, India, and Southeast Asia (20). Three clinical phenotypes of decreasing severity have been established: a transfusion-dependent state, thalassemia major, a moderate phenotype, thalassemia intermedia, and a benign heterozygous condition, thalassemia minor. In severe cases, the disease can be fatal in utero or in early childhood, if untreated. Clinical features, in addition to the RBC anomalies, are heterogeneous, and patients display several systemic manifestations.

Thromboembolic events such as pulmonary embolism, stroke, and thrombosis of the arterial and venous vascular beds are common complications reported in β-thalassemia major patients (1, 8). Possible vasoocclusive causes have been investigated and involve mainly functional and morphological erythrocyte abnormalities (22, 28). Indeed, thalassemic RBCs display markedly reduced cellular deformability compared with normal cells (23). In addition, erythrocytes from β-thalassemic patients exhibit enhanced cellular adhesion to each other (4) and to endothelial cells (10). A multifactorial chronic hypercoagulable state has also been widely recognized in thalassemic patients (7), and abnormalities of platelets and of the coagulation system may conceivably contribute to circulatory disorders. The exact underlying pathophysiology of these circulatory disorders remains to be documented.

The characterization of circulatory disorders per se in β-thalassemic patients is complicated by the various therapies that are likely to hinder hemodynamic assessment. Alternatively, important insights could be gained from untreated animal models. Several murine models of β-thalassemia have been generated through spontaneous or genetically induced mutations. One such model [$Hbb^{d3(th)/d3(th)}$] has been shown to closely reproduce hematological, pathological, and histological features of β-thalassemia major (26). Although this mouse model has existed for a long time, no previous studies on the vascular physiology or on the in vivo circulatory disturbances have been undertaken. One impediment to such progress has been the absence of noninvasive approaches to characterize blood flow. Herein we have thus established an ultrasound imaging approach to quantitatively assess microcirculatory disorders. In addition, we have investigated microcirculatory disorders without the confounding effect of treatments in β-thalassemic [$Hbb^{d3(th)/d3(th)}$] mice and determined that β-thalassemia can by itself lead to an impairment of vascular hemodynamic properties.

## METHODS

### *Mouse Strains*

Experimental procedures were approved by the Institutional Animal Care Committees of the Clinical Research Institute of Montreal and the University of Montreal Hospital Research Center, and they were conducted in compliance with the guidelines of the Canadian Council on Animal Care. Homozygous mice for a spontaneous mutation $Hbb^{d3(th)}$ were obtained by deletion of the murine β-major globin gene in the globin diffuse haplotype, leaving the β-globin minor gene intact (26). These homozygous β-thalassemic animals are severely affected (26). The thalassemic mice used in this study were

Article published online before print. See web site for date of publication (http://physiolgenomics.physiology.org).

Address for reprint requests and other correspondence: G. Cloutier, Laboratory of Biorheology and Medical Ultrasonics, Univ. of Montreal Hospital Research Center, 2099 Alexandre de Sève, Rm. Y-1619, Montreal, Quebec, Canada, H2L 2W5 (e-mail: guy.cloutier@umontreal.ca).

backcrossed for more than 16 generations onto C57BL/6J inbred mice to have a homogenous background. Congenic C57BL/6J control animals carry a globin single haplotype and were obtained from Jackson Laboratories (Bar Harbor, ME). All mice were maintained in microisolator cages.

### *Fetal Liver Transplantation*

Because of the severe thalassemic phenotype, a limited number of homozygous β-thalassemic mice were available at any one time. To circumvent this problem, we generated homozygous β-thalassemic fetuses (E14.5) from heterozygous β-thalassemic mating, and used fresh fetal liver as donor cells for transplantation. Fetal liver cells were obtained from three homozygous β-thalassemic fetal donors (C57BL/6J) and resuspended in serum-free Iscove's Modified Dulbecco's Medium (Gibco, Grand Island, NY). The C57BL/6J recipient mice were exposed to 875 cGy of total body irradiation (Mark I-68A-1 Research Irradiator, San Francisco, CA), and 2 h later, they received a total of $1.8 \times 10^6$ bone marrow cells suspended in a physiological solution of 350 μl injected into the tail vein. The transplanted mice were monitored on a regular basis for hematopoietic engraftment from 4 to 25 wk post-fetal liver cell transfer. Evaluation of engraftment was determined from peripheral blood on the basis of hemoglobin composition by the proportion of donor (Hb minor) and recipient (Hb single) hemoglobin. This assay involved loading RBC lysates onto cellulose acetate membranes (Titan III-H; Helena, Helena, CA) and electrophoresing for 35 min at 300 V in a Tris-borate-EDTA buffer (pH 8.5) using Helena equipment. Briefly, the protocol involved membrane staining with Ponceau S (Helena), destaining for 5 min in 5% acetic acid and 10 min in 100% ethanol, and fixation for 5 min in 70% methanol and 30% acetic acid, followed by drying for 6 min at 55°C. Sole expression of hemoglobin minor in C57BL/6J recipient mice demonstrated complete hematopoietic engraftment and confirmed production of homozygous β-thalassemic transplanted animals (homo-βthal).

### *Animal Preparation*

Seventeen male homo-βthal mice and nineteen C57BL/6J age-matched controls were studied. Mice were weighed and anesthetized using an intraperitoneal injection of 0.015 ml/g 2,2,2-tribromoethanol, 2.5%. The lumbar body hair was removed using a commercial depilatory cream (Nair, Church and Dwight, Princeton, NJ) applied over the anterior chest and neck of each animal. Mice were then placed on a warming platform under a heating lamp. The body temperature was monitored using a rectal thermometer (THM100; Indus Instruments, Houston, TX) and maintained to 37 ± 1°C. ECG electrodes on the platform supporting the mouse allowed us to continuously monitor the heart rate (HR). An estimate of mean aortic blood pressure (MBP) measurements was obtained using a tail-cuff monitoring system (XBP-1000; Kent Scientific, Torrington, CT) (13).

### *Echographic Examinations*

A high-resolution ultrasound biomicroscope (Vevo 660; Visualsonics, Toronto, ON, Canada) equipped with a single-element oscillating transducer (central frequency of 35 MHz, focal length of 10 mm, and frame rate of 30 Hz) was used. Lateral and axial resolutions for this probe are ~115 and ~55 μm, respectively (35). The axial dimension of the sample volume in pulsed-wave Doppler mode was fixed to 0.3 mm for recordings in the common carotid artery and to 0.51 mm for recordings in the ascending and abdominal aortas. Preheated ultrasound transmission gel (Aquasonic 100; Parker Laboratories, Orange, NJ) was placed on the regions of interest to provide an acoustic coupling medium between the probe and the animal.

The left common carotid artery and abdominal aorta were imaged longitudinally by B-mode ultrasonography at 35 MHz, and the Doppler sample volume was positioned precisely into the vessel of interest to record the time-varying velocity waveforms for 2 s. The Doppler recordings were performed at 30 MHz, 1–2 mm before the carotid bifurcation and above the renal bifurcation, identified by imaging the kidneys as reference.

The heart was imaged by using the B-mode parasternal long-axis view. The M-mode sampling line was positioned perpendicular to the ascending aorta at the exit of the left ventricle, and time-varying tracings were recorded to follow changes in aortic diameters (AoD). For Doppler recordings, the transducer was oriented to obtain an angle below 60° between the ultrasound beam and the aortic arch. The Doppler velocity waveforms were recorded in the ascending aorta by positioning the sampling volume at the exact same location where the M-mode tracings were obtained. An automatic angle correction provided by the instrument was applied to record quantitative velocity measures.

### *Hemodynamic Variables Measured Noninvasively*

*Pourcelot index.* Manual measurements using Matlab software (version 6.5, Natick, MA) were made of the peak systolic velocity (S) and of the end-diastolic velocity (D) in both common carotid artery and abdominal aorta (see Fig. 3). The Pourcelot index (PI) was calculated by use of the following formula (21)

$$PI = (S - D)/S$$

The mean PI value for each measurement was averaged over 10 consecutive cardiac cycles. A theoretical description of this index can be found in the APPENDIX.

*Stroke volume, cardiac output, and cardiac index.* The AoD was measured 0.5–1.5 mm downstream of the aortic valve in systole and diastole. An average value was then calculated over five cardiac cycles. The velocity-time integral (VTI) was determined by tracing manually the envelope of the Doppler velocity waveforms measured at the same location as AoD. VTI was averaged over 10 cardiac cycles. With the assumption of parabolic velocity profiles, the stroke volume (SV) was then calculated as follows

$$SV = \frac{1}{2}(AoD/2)^2 \times \pi \times VTI$$

The assumption of parabolic velocity profiles, and therefore the presence of 1/2 in the above equation, is justified, since the calculated Womersley number (15) in the ascending aorta was 2.5 on average in the present study. Because the measured Womersley number was small, we can assume Poiseuille parabolic-like flow in the ascending aorta of the studied mice. Moreover, velocity profiles have been shown to be parabolic in ascending aortas of rats (6).

Cardiac output (CO) was deduced from SV by multiplying it by the HR (CO = SV × HR). The cardiac index (CI) was finally calculated by normalizing CO for body weight and was expressed in milliliters per minute per gram of body weight ($ml \cdot min^{-1} \cdot g^{-1}$).

*Total peripheral vascular resistance.* Total peripheral vascular resistance (TPVR) was calculated as

$$TPVR = MBP/CO \approx TCP/CO$$

where MBP and TCP are the mean aortic blood pressure and the tail-cuff pressure, respectively. Because it has been shown that TCP is similar to MBP in mice (13), TCP can be adequately used for the estimation of TPVR. In the above equation, the postcapillary pressure was neglected and assumed to be zero.

### *Variability Analyses*

Intra- and interobserver and intersession variability analyses were performed for the basic echographic measures AoD, VTI, and PI on a subgroup of eight C57BL/6J mice. Intraobserver variability was assessed on the same echographic images by a single observer repeating the measurements on different days. The interobserver variability was determined on the same echographic images by having two observers within the same session performing these measurements. Intra- and interobserver errors were calculated as the difference between two measures divided by the mean and expressed as a percentage of variability. For the intersession variability, the echographic examinations were repeated on two different days at a 1-wk interval. Intersession variability was calculated as $(D_1 - D_7)/[(D_1 + D_7)/2]$, where $D_1$ and $D_7$ are two measurements performed by the same reader on the echographic images obtained in the sessions of the first and seventh days, respectively.

*Statistical Analyses*

Data were averaged and reported as means ± SE over *n* observations, where *n* represents the number of mice per group. Comparisons of results from homo-βthal and control mice were made by Student's unpaired *t*-tests. Statistical significance was considered at $P < 0.05$.

**RESULTS**

*Production of Homo-βthal Mice by Fetal Liver Cell Transplants*

The homozygous β-thalassemic [$Hbb^{d3(th)/d3(th)}$] mouse model was deleted for both adult β-globin major genes but had intact β-globin minor genes. Since a large population of homozygous β-thalassemic mice could not be obtained because of poor breeding efficiency, a strategy was developed to generate sufficient animal numbers. As described earlier, fetal liver cell transplants from three homozygous β-thalassemic mice were thus performed, conferring the entire spectrum of hematological defects from thalassemic donors to fetal liver recipients. Because recipients (Hb single) and donors (Hb minor) express alternative forms of hemoglobin, RBC engraftment was verified through the exclusive presence of the donor hemoglobin in recipient blood by 10–25 wk posttransplant, congruent with the clearance rate of normal murine RBCs. Figure 1 depicts the hemoglobin phenotype of five representative recipients 17 wk following the transplant. As expected, all transplanted animals produced strictly hemoglobin minor, the donor cell hemoglobin, which revealed complete fetal liver engraftment. Consistently, all transplanted mice were monitored for hematological parameters and showed severe anemia

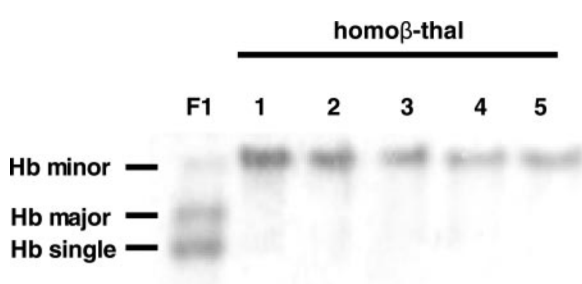


Fig. 1. Analysis of engraftment of fetal liver transplanted mice. Red blood cell hemoglobin levels in recipient mice were determined to evaluate engraftment of donor $Hbb^{d3(th)/d3(dth)}$ fetal liver cells (Hb minor) at 10 wk following transplantation. Protein electrophoresis of hemoglobin single from the globin single haplotype has fastest migrating band, as indicated, whereas the hemoglobin major and minor from the diffuse haplotype migrate slower. By 14 wk, recipients produced strictly hemoglobin minor, indicating a complete switch from hemoglobin single production and thus complete hematopoietic engraftment. Blood from C57BL/6J×CBA/J F1 mice (F1) served as control for single (Hb single) and diffuse (Hb major, Hb minor) haplotype. Homo-βthal, homozygous β-thalassemic transplanted.

Table 1. *Physiological and echographic parameters*

| Parameter | Control ($n$ = 19) | Homoβ-thal ($n$ = 17) | $P$ Value |
|---|---|---|---|
| Age, mo | 9.2±0.6 | 9.4±0.4 | NS |
| Body wt, g | 28.6±0.6 | 25.5±0.6 | <0.01 |
| AoD, mm | 1.49±0.02 | 1.41±0.02 | <0.05 |
| VTI, cm | 5.5±0.1 | 5.1±0.2 | NS |
| SV, ml/min | 0.048±0.001 | 0.041±0.003 | <0.01 |

Values are means ± SE. Homoβ-thal, homozygous β-thalassemic transplanted; AoD, aortic diameter; VTI, velocity-time integral of the aortic velocity; SV, stroke volume; NS, not significant.

with a hematocrit that ranged from 27 to 34%, whereas the hematocrit in normal mice of the same age was 49.0 ± 1.3%. Transplanted mice developed features identical to those of donor mice and consistent with severe β-thalassemia major.

At the time of echographic examinations, homo-βthal mice were 9.4 ± 0.4 mo old ($n$ = 17), and, as seen in Table 1, they were age matched to wildtype (WT) controls (9.2 ± 0.7 mo; $n$ = 19). Although all mice were of similar age, body weight was significantly decreased by ~10% ($P < 0.01$) in β-thalassemic animals (25.5 ± 0.6 g) relative to WT controls (28.6 ± 0.6 g), as frequently observed in humans with β-thalassemia major (5, 31).

Because ultrasound scans are difficult to accomplish in conscious mice, we resorted to general anesthesia despite its impact on cardiac function and hemodynamics (11, 34). However, we have limited the influence of anesthesia in our study by administering only the minimal dose granting a sufficient time period to perform echographic examinations. The comparisons between the two groups of mice were done under the same anesthetic regimen to avoid confounding effects.

*Increase of Global Vascular Resistance in β-Thalassemic Mice*

To investigate blood flow hemodynamics in β-thalassemia, systemic cardiovascular parameters were examined in untreated homo-βthal mice presenting features similar to those observed in β-thalassemia major patients. Although the MBP was slightly higher in homo-βthal mice (84.7 ± 3.9 mmHg) compared with WT mice (79.5 ± 3.6 mmHg), there was no statistical difference between the two groups ($P$ = 0.34, Fig. 2*A*). HR was determined from the ECG (Fig. 2*B*) and was also comparable between groups (483.7 ± 12.7 vs. 467.7 ± 7.5 beats/min, $P$ = 0.27). SV was 41 ± 3 and 48 ± 1 μl for homo-βthal and control mice, respectively ($P < 0.05$). The lower SV in homo-βthal mice likely results from their smaller body size, since SV values were similar when normalized to body weight ($P$ = 0.07). The CO and CI were not statistically different ($P$ = 0.07 and $P$ = 0.83, respectively) in both groups. As indicated in Fig. 2*C*, CI was 0.77 ± 0.05 $ml \cdot min^{-1} \cdot g^{-1}$ in homo-βthal mice compared with 0.79 ± 0.02 $ml \cdot min^{-1} \cdot g^{-1}$ in control mice. A significant increase of TPVR (Fig. 2*D*), by 30% ($P < 0.01$), was found in homo-βthal mice (4.65 ± 0.37 $mmHg \cdot min \cdot ml^{-1}$) compared with WT controls (3.58 ± 0.14 $mmHg \cdot min \cdot ml^{-1}$), which confirms general vascular blood flow anomalies in the β-thalassemic group.

*Impairment of Vascular Properties in Homo-βthal Mice*

Because β-thalassemic mice showed systemic circulatory disorders (according to TPVR), specific circulatory effects

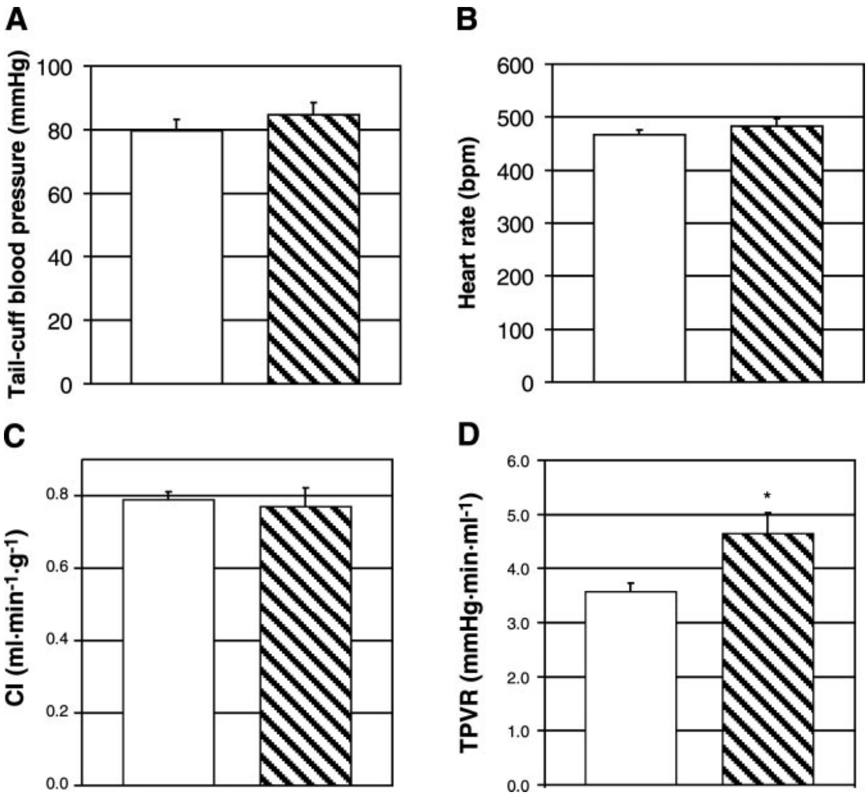


Fig. 2. Tail-cuff blood pressure (TCP, mmHg; *A*), heart rate (HR, beat/min; *B*), normalized cardiac output (CI, $ml \cdot min^{-1} \cdot g^{-1}$; *C*), and total peripheral vascular resistance (TPVR, $mmHg \cdot min \cdot ml^{-1}$; *D*) in homo-βthal ($n$ = 17, hatched bars) and control ($n$ = 19, open bars) mice. Data are means ± SE. *$P < 0.01$.

were further investigated by Doppler ultrasonography. Two different and complementary sites were selected to evaluate vascular properties: the carotid artery feeding the brain and the abdominal aorta irrigating major organs and the lower limbs. The rationale for selecting the left common carotid relied on the fact that cerebral thromboembolic events have been documented in β-thalassemic patients (1, 7). The abdominal aorta was also chosen because it is easily accessible and it is the main supplier of blood flow to numerous organs and tissues, including the kidneys, where anomalies were described in humans (1).

PI was calculated as is done for human radiology scans. Using the ultrasound biomicroscope, we measured the Doppler peak systolic and end-diastolic velocities (as in Fig. 3) to derive PI in the carotid artery and abdominal aorta. The diameter of both vessels was large enough to allow accurate and reproducible localization of the Doppler recording sites, as shown by the white arrow in Fig. 4*A* for the smallest vessel investigated in this study (the carotid). As reported in Fig. 5, PI was significantly higher in the homo-βthal group for both vessels. In the common carotid artery, PI was 0.867 ± 0.007 (no units) in homo-βthal mice compared with 0.832 ± 0.007 in control mice ($P < 0.01$), whereas those values were 0.822 ± 0.012 in homo-βthal and 0.792 ± 0.008 in control mice for the abdominal aorta ($P < 0.05$). This increase of PI in the β-thalassemic group was directly related to a decrease in diastolic blood flow velocity, as shown in Fig. 4, *B* and *C*. These results suggest that the homo-βthal mice had impaired vascular properties in the neck vessels, abdomen, and lower limbs.

### *PI Measurements Are Reproducible with Low Interpretive Variabilities*

To validate the noninvasive echographic approaches reported in this study, the reproducibility of most measures was verified by computing the intra- and interobserver and intersession variabilities. As indicated in Table 2, the largest vari-

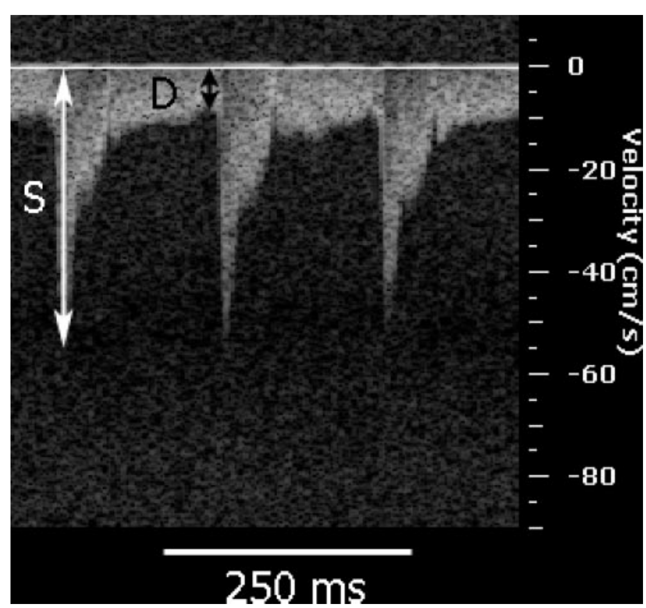


Fig. 3. Doppler display of common carotid artery velocity waveforms of a wildtype mouse showing the systolic (S) and end-diastolic (D) velocities. Three cardiac cycles are displayed.

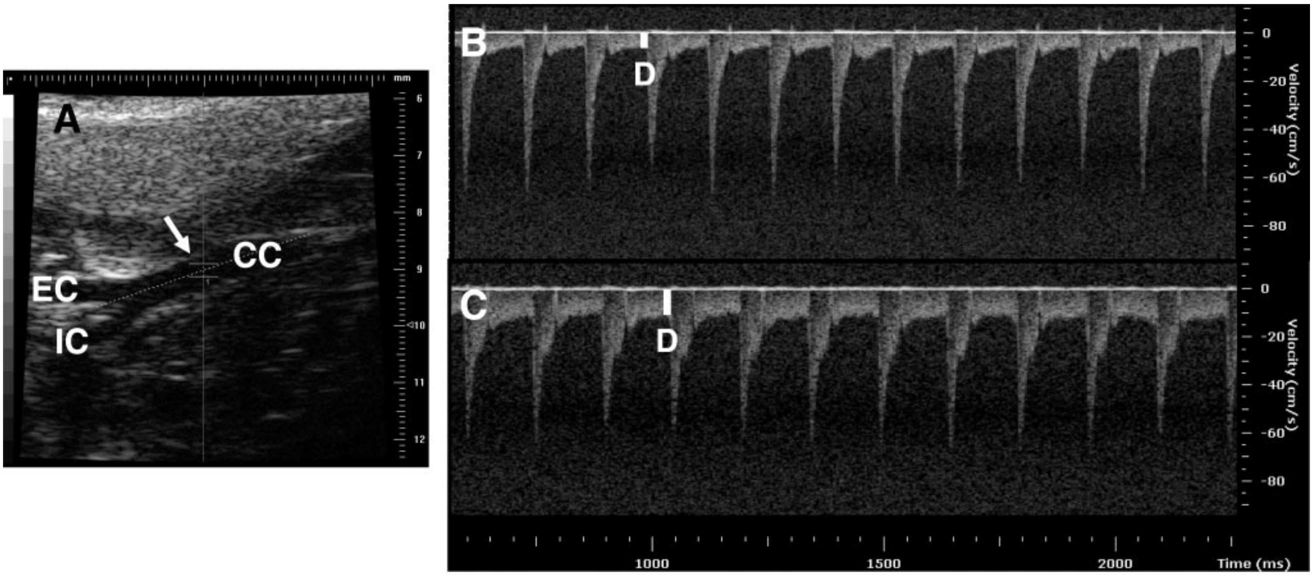


Fig. 4. Ultrasonographic imaging of the carotid artery. *A*: B-mode image showing the common carotid artery (CC) and the internal (IC) and external (EC) carotid arteries in longitudinal view. The Doppler sample volume (white arrow) is positioned within the CC artery before the bifurcation. *B* and *C*: Doppler flow velocity waveforms recorded in the CC artery of a β-thalassemic mouse (*B*) and same measures in a wildtype control mouse (*C*). D, end-diastolic velocity (white line).

ability was observed for VTI, but it did not exceed 10% even when evaluated by different observers. The intra- and interobserver absolute errors for CO and TPVR were low at 2.8 ± 4.0% and 1.0 ± 5.0%, respectively. Noticeably, intra- and interobserver variabilities on PI were <1%. Similarly, for the intersession variability assessment reported in Table 3, all measurements were quite reproducible when performed at an interval of 1 wk. Of all measures, CO (−11.1 ± 6.2%) and TPVR (12.6 ± 8.2%) appeared the most variable. By contrast, even when performed on different recording sessions, PI measurements were highly reproducible with an error of 1.7 ± 1.8% for the carotid artery and 2.1 ± 2.6% for the abdominal aorta. Of all noninvasive variables used to assess hemodynamic impairments in homo-βthal mice, PI was the most reliable.

## DISCUSSION

The purpose of this study was to investigate the presence of blood flow abnormalities in the peripheral circulation of β-thalassemic mice, with a secondary objective of developing noninvasive imaging tools for the assessment of cardiovascular disorders. Using a novel ultrasound diagnostic approach, we have demonstrated circulatory flow disorders in homo-βthal mice.

Herein, we produced homo-βthal mice that displayed a phenotype typical of human β-thalassemia major, with a pronounced β- to α-globin chain imbalance, for hemodynamic analysis. While no difference was noted in standard cardiovascular parameters such as the cardiac index, heart rate and mean blood pressure, significant blood flow changes were obtained in homo-βthal animals by measuring the total peripheral vascular resistance. Such flow alterations in homo-βthal mice were also observed on local flow waveforms, as determined by the PI. In human, PI derived from the Doppler waveform is a well-recognized parameter for the assessment of vascular hemodynamics. Hence, this study proposed a novel use of this parameter for the noninvasive evaluation of cardiovascular physiology in mice. The high-frequency ultrasound biomicroscope allowed accurate and reproducible Doppler flow velocity measurements in all animals and overcame the limitations of

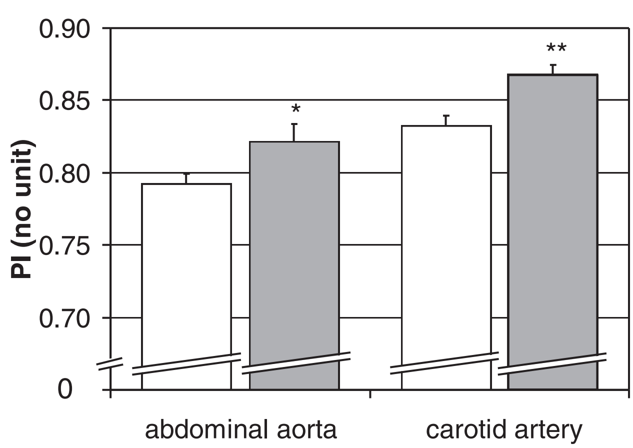


Fig. 5. Doppler Pourcelot indexes (PI, no units) in the common carotid artery and abdominal aorta of homo-βthal ($n$ = 17, shaded bars) and control ($n$ = 19, open bars) mice. Data are means ± SE. *$P < 0.05$; **$P < 0.01$.

Table 2. *Intra- and interobserver variabilities of echographic measurements*

| Parameter | Intraobserver Variability, % | Interobserver Variability, % |
|---|---|---|
| AoD, mm | 0.7±0.5 | −0.2±0.5 |
| VTI, cm | −4.3±1.4 | −8.1±0.9 |
| CO, ml/min | 2.8±4.0 | −1.0±5.0 |
| TPVR, mmHg·min·ml$^{-1}$ | −2.8±4.0 | 1.0±5.0 |
| PI (no units) | | |
| Carotid artery | 0.3±0.2 | 0.7±0.4 |
| Abdominal aorta | −0.2±0.3 | 0.9±0.3 |

Values are means ± SE; $n$ = 8 wildtype control mice. Intra- and interobserver variabilities were calculated as the difference of 2 measures performed on the same image divided by the mean of those 2 measurements expressed as a percentage. CO, cardiac output; TPVR, total peripheral vascular resistance; PI, Pourcelot index.

Table 3. *Intersession variability of the echographic parameters*

| Parameter | % of Error |
|---|---|
| AoD, mm | $-5.4 \pm 2.3$ |
| VTI, cm | $6.7 \pm 4.7$ |
| CO, ml/min | $-11.1 \pm 6.2$ |
| TPVR, mmHg·min·ml$^{-1}$ | $12.6 \pm 8.2$ |
| PI (no units) | |
| Carotid artery | $1.7 \pm 1.8$ |
| Abdominal aorta | $2.1 \pm 2.6$ |

Values are means ± SE; $n$ = 8 wildtype control mice. Intersession variability errors were calculated as the difference between the measurements performed by the same reader on the images obtained during 2 different scanning sessions separated by a 7-day interval.

clinical ultrasound scanners (having a much lower spatial resolution and a larger probe head).

When compared with the total peripheral vascular resistance, PI provides alternative information on systemic hemodynamics and presents major advantages. Indeed, PI is highly reproducible and is more time efficient. Thus PI has considerable appeal as a means to evaluate noninvasively vascular impairment in mice. We showed from the pi (Π)-theorem that PI is mainly related to the diastolic decay time measured at a specific location along the vascular tree. It should be noted that the Π-theorem is unable to provide a complete theoretical description of PI. According to the theoretical background provided in the APPENDIX, one can just state that PI is governed by the diastolic decay time normalized by the cardiac period when some physiological parameters such as the blood density and the cross-sectional area of the vessel are given. A more complete theoretical analysis is not straightforward and would require a series of numerical or analytical simulations in a complex model of the blood circulation. In this study, because the heart rate did not significantly differ from one group to another, we can only assert that PI was related to the so-called diastolic decay time (in a linear way or not) for measurements in the ascending aorta and carotid artery. The diastolic decay time can be defined as the product of the local arterial compliance by the downstream vascular resistance, as in the Windkessel model. However, we cannot confirm this if one considers the numerous limitations of this last model (17).

An interesting finding was the fact that PI varied with the site of measurement. This was predictable, since, besides resistance and compliance, it is highly dependent on the cross-sectional area of the vascular bed downstream of the site of examination (2). Surprisingly, when compared with human physiology, we observed higher values of PI in the carotid (brain vascular network) than in the abdominal aorta (renal, abdominal, and lower limb vascular network) of mice. Because the flow waveform changes along the abdominal aorta, we noted that a small variation in the site of measurement could lead to high differences in PI values. Therefore, we defined, using B-mode imaging, a precise localization of the Doppler sample volume, just above the renal bifurcations, to ensure reproducible measurements.

An increase in vascular resistance to blood flow should theoretically be primarily determined by direct changes in arteriolar diameters (19) and by alterations of the normal erythrocyte function, which is essential for the adequate flowing of blood in the macro- and microcirculation (24). In our homo-βthal mice, the increase in vascular resistance potentially results from alterations of the endothelium of blood vessels, a critical regulator of the vascular tone. The altered membrane composition of erythrocytes affecting their function, due to the precipitation of excess α-globin chains, may have also resulted in enhanced adherence of RBCs to endothelial cells and abnormal RBC aggregation increasing blood viscosity. Consequently, thromboembolic complications, as reported in β-thalassemic patients (14, 23, 25), may explain the increased flow resistance in pathological β-thalassemic mice.

In summary, we have demonstrated the feasibility of performing noninvasive measurements of vascular hemodynamic properties by high-frequency ultrasonography in mice. Our results also showed, for the first time, in vivo evidence of flow disorders in β-thalassemic mice. The imaging approach, as developed in this study, will open the field of noninvasive circulatory investigation to additional mouse models and to dissection of the contribution of molecular and cellular modulators of flow. Importantly, our findings will not only be very pertinent for assessing vascular pathophysiology phenotype but also will provide crucial criteria for evaluating genetic treatment efficiency in β-thalassemia and other diseases impairing the flow of blood.

## APPENDIX

### *PI: Theoretical Background*

The PI is a dimensionless echographic parameter commonly used to characterize vascular hemodynamics downstream of an artery. PI depends on both the arterial compliance (C) and downstream vascular resistance (R) (3). It still remains unknown how these two variables mathematically relate to PI. A simple dimensional analysis may, however, help to better understand how PI varies with vascular parameters.

The arterial flow waveform is mainly characterized by the cardiac period (T), the mean flow rate, the arterial cross-sectional area, the blood density and viscosity, the pulse wave velocity along the artery, the wave reflection at bifurcations and at sites of vessel caliber changes, and parameters R and C. The pulse wave velocity is affected by C and the blood density (16). On the other hand, the wave reflection depends on the cross-sectional area and pulse wave velocity (12). In addition, with the assumption that mean flow rate, arterial cross-sectional area, blood density, and viscosity have fixed values in a given animal, the Π-theorem (27) allows one to write PI as a function of $R \times C \div T$. The product $R \times C$ is the diastolic decay time, and it characterizes the rate at which pressure inside an artery decays during diastole. This parameter reflects the mechanical behavior of the vascular tree, and it has been used in both animals and patients (18, 33). The lower the PI and the higher the diastolic decay time, then, physiologically, the better the mechanical vascular property.

## ACKNOWLEDGMENTS

We thank Erick Raymond-Beaubien for contributions to the interobserver variability study and the Foundation of the University of Montreal Hospital for the purchase of the Visualsonics high-frequency ultrasound system.

## GRANTS

This work was supported by the Canadian Institute of Health Research (CIHR Grants MOP-36467, to G. Cloutier, and MOP-67233, to M. Trudel) and through joint funding to G. Cloutier and M. Trudel by National Heart, Lung, and Blood Institute Grant RO1-HL-078655, CIHR Grant CMI-72323, and Heart and Stroke Foundation of Canada Grant PG-05-0313. G. Cloutier is the recipient of the National Scientist Award of the "Fonds de la Recherche en

Santé du Québec" (2004–2009). H. Felfly is supported by a studentship from the "Programme Canadien des Bourses de la Francophonie."

## REFERENCES

1. **Borgna PC, Carnelli V, Caruso V, Dore F, De Mattia D, Di Palma A, Di Gregorio F, Romeo MA, Longhi R, Mangiagli A, Melevendi C, Pizzarelli G, Musumeci S.** Thromboembolic events in beta thalassemia major: an Italian multicenter study. *Acta Haematol* 99: 76–79, 1998.
2. **Bude RO, Rubin JM.** Effect of downstream cross-sectional area of an arterial bed on the resistive index and the early systolic acceleration. *Radiology* 212: 732–738, 1999.
3. **Bude RO, Rubin JM.** Relationship between the resistive index and vascular compliance and resistance. *Radiology* 211: 411–417, 1999.
4. **Chen S, Eldor A, Barshtein G, Zhang S, Goldfarb A, Rachmilewitz E, Yedgar S.** Enhanced aggregability of red blood cells of beta-thalassemia major patients. *Am J Physiol Heart Circ Physiol* 270: H1951–H1956, 1996.
5. **Cheung YF, Ha SY, Chan GCF.** Ventriculo-vascular interactions in patients with (beta) thalassaemia major. *Heart* 91: 769–773, 2005.
6. **Doursout MF, Wouters P, Kashimoto S, Hartley CJ, Rabinovitz R, Chelly JE.** Measurement of cardiac function in conscious rats. *Ultrasound Med Biol* 27: 195–202, 2001.
7. **Eldor A, Rachmilewitz EA.** The hypercoagulable state in thalassemia. *Blood* 99: 36–43, 2002.
8. **Gillis S, Cappellini MD, Goldfarb A, Ciceri L, Fiorelli G, Rachmilewitz EA.** Pulmonary thromboembolism in thalassemia intermedia patients. *Haematologica* 84: 959–960, 1999.
9. **Hoffman R.** *Hematology: Basic Principles and Practice*. New York: Churchill-Livingstone, 2005.
10. **Hovav T, Goldfarb A, Artmann G, Yedgar S, Barshtein G.** Enhanced adherence of beta-thalassaemic erythrocytes to endothelial cells. *Br J Haematol* 106: 178–181, 1999.
11. **Janssen BJA, De Celle T, Debets JJM, Brouns AE, Callahan MF, Smith TL.** Effects of anesthetics on systemic hemodynamics in mice. *Am J Physiol Heart Circ Physiol* 287: H1618–H1624, 2004.
12. **Khir AW, Parker KH.** Measurements of wave speed and reflected waves in elastic tubes and bifurcations. *J Biomech* 35: 775–783, 2002.
13. **Krege JH, Hodgkin JB, Hagaman JR, Smithies O.** A noninvasive computerized tail-cuff system for measuring blood pressure in mice. *Hypertension* 25: 1111–1115, 1995.
14. **Kuypers FA, Yuan J, Lewis RA, Snyder LM, Kiefer CR, Bunyaratvej A, Fucharoen S, Ma L, Styles L, Jong K, Schrier SL.** Membrane phospholipid asymmetry in human thalassemia. *Blood* 91: 3044–3051, 1998.
15. **Loudon C, Tordesillas A.** The use of the dimensionless Womersley number to characterize the unsteady nature of internal flow. *J Theor Biol* 191: 63–78, 1998.
16. **Mackenzie IS, Wilkinson IB, Cockcroft JR.** Assessment of arterial stiffness in clinical practice. *QJM* 95: 67–74, 2002.
17. **Milnor WR.** *Hemodynamics.* Baltimore, MD: Williams and Wilkins, 1989.
18. **Molino P, Cerutti C, Julien C, Cuisinaud G, Gustin MP, Paultre C.** Beat-to-beat estimation of windkessel model parameters in conscious rats. *Am J Physiol Heart Circ Physiol* 274: H171–H177, 1998.
19. **Nichols WW, O'Rourke MF.** *McDonald's Blood Flow in Arteries: Theoretical, Experimental and Clinical Principles*. London: Oxford Univ. Press, 1998.
20. **Olivieri NF.** The beta-thalassemias. *N Engl J Med* 341: 99–109, 1999.
21. **Pourcelot L.** Indications of Doppler's ultrasonography in the study of peripheral vessels. *Revue du Praticien* 25: 4671–4680, 1975.
22. **Schrier SL.** Pathophysiology of thalassemia. *Curr Opin Hematol* 9: 123–126, 2002.
23. **Schrier SL, Rachmilewitz E, Mohandas N.** Cellular and membrane properties of alpha and beta thalassemic erythrocytes are different: implication for differences in clinical manifestations. *Blood* 74: 2194–2202, 1989.
24. **Shiga T, Maeda N, Kon K, Shiga T, Maeda N, Kon K.** Erythrocyte rheology. *Crit Rev Oncol Hematol* 10: 9–48, 1990.
25. **Shinar E, Shalev O, Rachmilewitz EA, Schrier SL.** Erythrocyte membrane skeleton abnormalities in severe beta-thalassemia. *Blood* 70: 158–164, 1987.
26. **Skow LC, Burkhart BA, Johnson FM, Popp RA, Popp DM, Goldberg SZ, Anderson WF, Barnett LB, Lewis SE.** A mouse model for beta-thalassemia. *Cell* 34: 1043–1052, 1983.
27. **Sonin AA.** A generalization of the (Pi)-theorem and dimensional analysis. *Proc Natl Acad Sci USA* 101: 8525–8526, 2004.
28. **Sorensen S, Rubin E, Polster H, Mohandas N, Schrier S.** The role of membrane skeletal-associated alpha-globin in the pathophysiology of beta-thalassemia. *Blood* 75: 1333–1336, 1990.
29. **Stamatoyannopoulos G, Majerus PW, Perlmutter RM, Varmus H.** *The Molecular Basis of Blood Diseases*. Philadelphia, PA: WB Saunders, 2001, p. 183–273.
30. **Tuzmen S, Schechter AN.** Genetic diseases of hemoglobin: diagnostic methods for elucidating beta-thalassemia mutations. *Blood Rev* 15: 19–29, 2001.
31. **Vaccari M, Crepaz R, Fortini M, Gamberini MR, Scarcia S, Pitscheider W, Bosi G.** Left ventricular remodeling, systolic function, and diastolic function in young adults with (beta)-thalassemia intermedia: a Doppler echocardiography study. *Chest* 121: 506–512, 2002.
32. **Weatherall DJ.** Phenotype-genotype relationships in monogenic disease: lessons from the thalassaemias. *Nat Rev Genet* 2: 245–255, 2001.
33. **Westerhof N, Elzinga G.** Normalized input impedance and arterial decay time over heart period are independent of animal size. *Am J Physiol Regul Integr Comp Physiol* 261: R126–R133, 1991.
34. **Yang XP, Liu YH, Rhaleb NE, Kurihara N, Kim HE, Carretero OA.** Echocardiographic assessment of cardiac function in conscious and anesthetized mice. *Am J Physiol Heart Circ Physiol* 277: H1967–H1974, 1999.
35. **Zhou YQ, Foster FS, Nieman BJ, Davidson L, Chen XJ, Henkelman RM.** Comprehensive transthoracic cardiac imaging in mice using ultrasound biomicroscopy with anatomical confirmation by magnetic resonance imaging. *Physiol Genomics* 18: 232–244, 2004.